JACC: CARDIOVASCULAR IMAGING VOL. 3, NO. 9, 2010

ISSN 1936-878X/$36.00
PUBLISHED BY ELSEVIER INC. DOI:10.1016/j.jcmg.2010.06.013

Molecular Imaging of Activated von Willebrand Factor to Detect High-Risk Atherosclerotic Phenotype

Owen J. T. McCarty, PhD,*† Robert B. Conley, BS,* Weihui Shentu, MD,‡ Garth W. Tormoen, MS,* Daogang Zha, MD,‡ Aris Xie, BS,‡ Yue Qi, MD,‡ Yan Zhao, MD,‡ Chad Carr, MD,‡ Todd Belcik, RDCS,‡ Douglas R. Keene, BS,§ Philip G. de Groot, PhD,‖ Jonathan R. Lindner, MD,*‡

Portland, Oregon; and Utrecht, the Netherlands

OBJECTIVES We hypothesized that noninvasive molecular imaging of activated von Willebrand factor (vWF) on the vascular endothelium could be used to detect a high-risk atherosclerotic phenotype.

BACKGROUND Platelet-endothelial interactions have been linked to increased inflammatory activation and prothrombotic state in atherosclerosis. These interactions are mediated, in part, by platelet glycoprotein (GP) Ibα, suggesting that dysregulated endothelial vWF is a marker for high-risk atherosclerotic disease.

METHODS Microbubbles targeted to activated vWF were prepared by surface conjugation of recombinant GPIbα. Flow-chamber studies were used to evaluate attachment of targeted microbubbles to immobile platelet aggregates bearing activated vWF. Contrast-enhanced ultrasound (CEU) molecular imaging of the aorta from mice was performed: 1) ex vivo after focal crush injury and blood perfusion; and 2) in vivo in mice with advanced atherosclerosis produced by deletion of the low-density lipoprotein receptor and ApoBec-1 editing peptide (LDLR$^{-/-}$/ApoBec-1$^{-/-}$).

RESULTS In flow-chamber studies, tracer attachment to vWF was >10-fold greater for microbubbles bearing GPIbα compared with control microbubbles ($p < 0.01$). In the ex vivo aortic injury model, CEU signal enhancement for vWF-targeted microbubbles occurred primarily at the injury site and was 4-fold greater than at noninjured sites ($p < 0.05$). In LDLR$^{-/-}$/ApoBec-1$^{-/-}$ mice, inflammatory cell infiltrates and dense vWF expression on the intact endothelium were seen in regions of severe plaque formation. Scanning electron microscopy demonstrated widespread platelet-endothelial interaction and only few sites of endothelial erosion. On CEU, signal enhancement for vWF-targeted microbubbles was approximately 4-fold greater ($p < 0.05$) in LDLR$^{-/-}$/ApoBec-1$^{-/-}$ compared with wild-type mice. En face aortic microscopy demonstrated regions where platelet adhesion and microbubble attachment colocalized.

CONCLUSIONS Molecular imaging using GPIbα as a targeting moiety can detect the presence of activated vWF on the vascular endothelium. This strategy may provide a means to noninvasively detect an advanced prothrombotic and inflammatory phenotype in atherosclerotic disease. (J Am Coll Cardiol Img 2010;3:947–55) © 2010 by the American College of Cardiology Foundation

From the *Division of Biomedical Engineering, Oregon Health & Science University, Portland, Oregon; †Department of Cell & Developmental Biology, Oregon Health & Science University, Portland, Oregon; ‡Division of Cardiovascular Medicine, Oregon Health & Science University, Portland, Oregon; §Micro-Imaging Center, Shriners Hospitals for Children, Portland, Oregon; and the ‖Department of Clinical Chemistry and Haematology, University Medical Center Utrecht, Utrecht, the Netherlands. Supported by grants from the Oregon Clinical & Translational Institute and the Wallace Coulter Foundation Grant to Drs. McCarty and Lindner. Dr. de Groot is supported by a Dutch Heart Foundation grant. Dr. Lindner is supported by grants R01-HL078610, R01-HL074443, and R01-DK063508, and RC01-100659 from the National Institutes of Health. All other authors report that they have no relationships to disclose.

Manuscript received February 18, 2010; revised manuscript received June 21, 2010, accepted June 30, 2010.

JACC: CARDIOVASCULAR IMAGING, VOL. 3, NO. 9, 2010
SEPTEMBER 2010:947–55

Targeted imaging probes for noninvasive imaging of vascular phenotypes are being developed to evaluate an atherosclerotic profile. This approach may be useful for identifying high-risk patients or lesions and for guiding management. Molecular imaging strategies for evaluating an atherosclerotic phenotype broadly include those that evaluate inflammation, oxidized lipid content, protease activation, plaque neovascularization, or thrombus, all of which are interrelated through common cellular and molecular mediators.

See page 956

In this study, we hypothesized that molecular imaging of von Willebrand factor (vWF) in its activated state with targeted contrast ultrasound could be used to detect a high-risk and prothrombotic atherosclerotic phenotype. Platelet recruitment and adhesion is initiated by the interaction of platelet glycoprotein (GP) Ib-IX-V complex with the A1-domain of vWF that has undergone conformational activation (1,2). Activation of vWF is promoted by attachment to matrix proteins, high shear stress, or dysregulated vWF multimerization, all of which may occur in atherosclerosis (1–4). Hence targeted imaging of activated vWF could detect the inaugural events that lead to thrombotic complications of atherosclerosis or to detect an inflammatory milieu since transient platelet adhesion promotes endothelial activation (4,5). In this study, the use of recombinant GPIb as a targeting moiety on microbubble contrast agents is particularly advantageous for promoting attachment in high-shear vessels because GPIb subunit binding to vWF is characterized by "catch-bond" kinetics (2). To test our hypothesis, we used flow-chamber experiments to characterize attachment of targeted microbubbles to activated vWF. Contrast-enhanced ultrasound (CEU) molecular imaging was performed in ex vivo models of endothelial injury and microthrombus formation and in vivo in a murine model of advanced atherosclerosis.

ABBREVIATIONS AND ACRONYMS

CEU = contrast-enhanced ultrasound

DiO = dioctadecyloxacarbocyannine perchlorate

FITC = fluorescein isothiocyanate

GP = glycoprotein

LDLR$^{-/-}$/ApoBec-1$^{-/-}$ = low-density lipoprotein receptor and ApoBec-1–deficient mice

MI = mechanical index

PITA = pixel-intensity threshold analysis

vWF = von Willebrand factor

METHODS

Targeted microbubble preparation. Biotinylated, lipid-shelled decafluorobutane microbubbles were prepared as previously described (6). Recombinant human GPIbα, representing amino acids 1 to 290 (32.3 kD) of GPIb, was used as a targeting moiety. The peptide was biotinylated and conjugated to biotinylated microbubbles via a streptavidin link as previously described (6). For flow-chamber attachment studies, microbubbles were fluorescently labeled with dioctadecyl-tetramethylindocarbocyanine perchlorate or dioctadecyloxacarbocyannine perchlorate (DiO). The mean diameter of microbubbles on electrozone analysis (Multisizer III, Beckman Coulter Inc, Fullerton, California) was 1.9 to 2.4 μm and was not significantly different between preparations.

Flow-chamber adhesion. Glass capillary tubes were coated with fibrillar collagen by incubation with 100 μg/ml of collagen (Chrono-Log, Havertown, Pennsylvania) and were blocked with bovine serum albumin. The tubes were placed in a flow chamber mounted on an upright microscope with a ×40 objective (7). Whole blood collected from healthy volunteers was anticoagulated with corn trypsin inhibitor (40 μg/ml) and was infused through the tubes for 3 min at a shear rate of 500 s^{-1}. Either vWF-targeted or control microbubbles (5×10^6 ml^{-1}) suspended in 4-(2-hydroxyethyl)-1-piperazineethanesulfonic acid–Tyrode buffer were infused at a shear rate of 300 s^{-1} for 3 min followed by a 4-min wash. The density of microbubble adhesion in 10 optical fields (0.3 mm^2) was determined using phase-contrast and fluorescent microscopy.

Targeted imaging ex vivo. The study was approved by the Animal Care and Use Committee of the Oregon Health & Science University. The descending aorta from 20- to 30-week-old C57Bl/6 mice (n = 8) was removed, and the lumen was cannulated at each end. A mild crush injury 3 mm in length was made in the mid portion of the aorta. Whole blood anticoagulated with heparin (10 U/ml) was infused through the aorta for 5 min at a shear rate of 500 s^{-1}. Targeted or control microbubbles (1×10^6/ml) suspended in a 1:4 dilution of whole blood in phosphate buffered saline was infused for 5 min followed by a 3-min wash. CEU (Contrast-Pulse Sequencing, Sequoia; Siemens Medical Systems, Mountain View, California) was performed at 7 MHz using a long-axis imaging plane. Images were acquired using low-power imaging at a mechanical index (MI) of 0.16 before and after a brief high-MI (1.9) destructive frame sequence. Several high-frequency (14 MHz) B-mode images were also captured for anatomic reference. Data were analyzed as previously described to eliminate signal contribution from nonretained agent (6). At the injury and remote noninjured sites, acoustic signal enhancement was measured, and the

percentage of pixels demonstrating signal enhancement was determined using an automated pixel-intensity threshold analysis (PITA) using a threshold 3 SDs greater than the mean pre-contrast intensity (8).

Immunohistology for platelet adhesion. In 4 aortas undergoing ex vivo crush injury and blood infusion, 50 μg/ml of fluorescein isothiocyanate (FITC)–labeled rat anti-mouse platelet monoclonal antibody (MWReg30; BD Biosciences, San Jose, California) or FITC-labeled nonspecific monoclonal antibody (R3-34, BD Pharmingen) was infused into the aorta. The endothelial surface was imaged en face by fluorescent microscopy (Axioscop2-FS; Carl Zeiss, Thornburg, New York) with a silicon-intensified tube camera (SIT68; Dage-MTI, Michigan City, Indiana).

In vivo targeted imaging of atherosclerosis. Control wild-type C57Bl/6 mice and mice with genetic deletion of the low-density lipoprotein receptor and ApoBec-1 mRNA editing peptide ($LDLR^{-/-}$/$ApoBec\text{-}1^{-/-}$) (9) were studied at 40 weeks of age (n = 7 each). Mice were anesthetized with inhaled isoflurane, and a cannula was placed in a jugular vein. The ascending aorta and arch were imaged in long axis from a right parasternal imaging plane. Control and vWF-targeted microbubbles (1×10^6) were injected intravenously. CEU with each agent was performed 7 min after injection. Several frames were obtained with high-power (MI 1.2) imaging. Microbubbles in the sector were then fully destroyed by imaging at an MI of 1.9, and several post-destructive frames were obtained at an MI of 1.2 and a pulsing interval of 1 s. A single image reflecting only retained microbubbles was created by digitally subtracting several averaged post-destructive frames from the first pre-destruction frame. Intensity measurement and PITA analysis were performed from a region of interest placed around the ascending aorta and arch guided by fundamental imaging at 14 MHz. In additional mice ($LDLR^{-/-}$/$ApoBec\text{-}1^{-/-}$ and wild type), platelets were labeled in vivo by intravenous injection of rhodamine-6G (25 μg) followed by injection of 1×10^7 DiO-labeled vWF-targeted microbubbles. The aorta was removed after 5 min, and en face dual-fluorescent microscopy was used to evaluate colocalization of platelets with microbubbles.

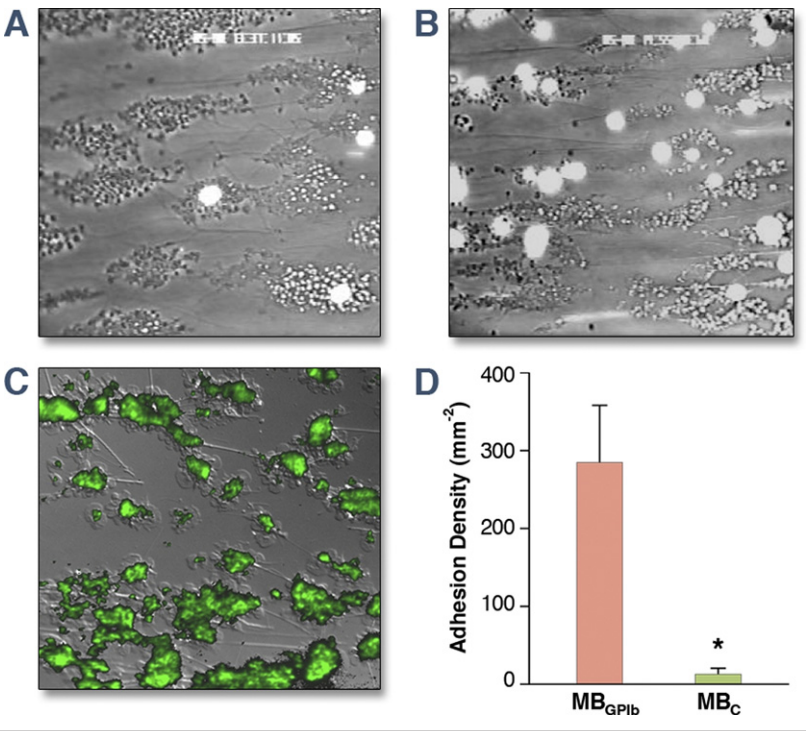

Figure 1. Attachment of vWF-Targeted Microbubbles to Thrombi Under Shear

Examples illustrating binding of fluorescently-labeled control **(A)** and von Willebrand factor (vWF)–targeted **(B)** microbubbles to platelet-rich thrombus in the flow chamber. **(C)** Fluorescent immunohistology demonstrating surface-bound vWF (fluorescein isothiocyanate–positive staining) in regions of microthrombus formation. **(D)** Mean (± standard error of the mean) density of attachment for vWF-targeted (MB_{GPIb}) or control (MB_c) microbubbles under shear (500 s^{-1}). *$p < 0.01$ compared with MB_{GPIb}. Raw data available in Online Figure 1.

Histology and immunohistochemistry. Immunohistochemistry for vWF was performed in the collagen-coated capillary tubes and perfusion-fixed aortas from 3 $LDLR^{-/-}$/$ApoBec\text{-}1^{-/-}$ and 3 wild-type mice. Movat's pentachrome stain was performed for assessment of plaque morphometry. Immunohistochemistry for vWF expression was performed with a rabbit polyclonal primary antibody (Ab6994; Abcam, Cambridge, Massachusetts), and secondary antibodies were either FITC-labeled (capillary tubes) or biotinylated (aortas) with secondary peroxidase staining (ABC Vectastain Elite; Vector Laboratories, Burlingame, California). Control experiments were performed with secondary antibody alone.

Electron microscopy. The aorta was collected from a wild-type and 2 $LDLR^{-}$/$ApoBec\text{-}1^{-}$ mice and fixed in Dulbecco's Modified Eagle Medium buffer containing 1.5% glutaraldehyde and 1.5% paraformaldehyde, then post-fixed in 1% Osmium tetroxide. Samples were dehydrated in a graded series of ethanol to 100%, rinsed in tetramethyl silane, and air dried. Samples were sputter-coated with gold palladium, and the luminal surface was observed by scanning electron microscopy (DS-130, ISI/TOPCON, Tokyo, Japan) operated at 10 KV.

Statistical analysis. Data were analyzed using RS/1 (Domain Manufacturing Corp., Burlington, Massachusetts). One-way analysis of variance was performed for normally distributed variables with post-hoc testing of individual comparisons with paired or unpaired *t* test. Bonferroni correction was applied for multiple comparisons. Nonparametric data were compared with the Mann-Whitney rank-sum test. Values of $p < 0.05$ were considered to be statistically significant.

RESULTS

In vitro molecular imaging of activated vWF. In capillary tubes coated with fibrillar collagen, a thin

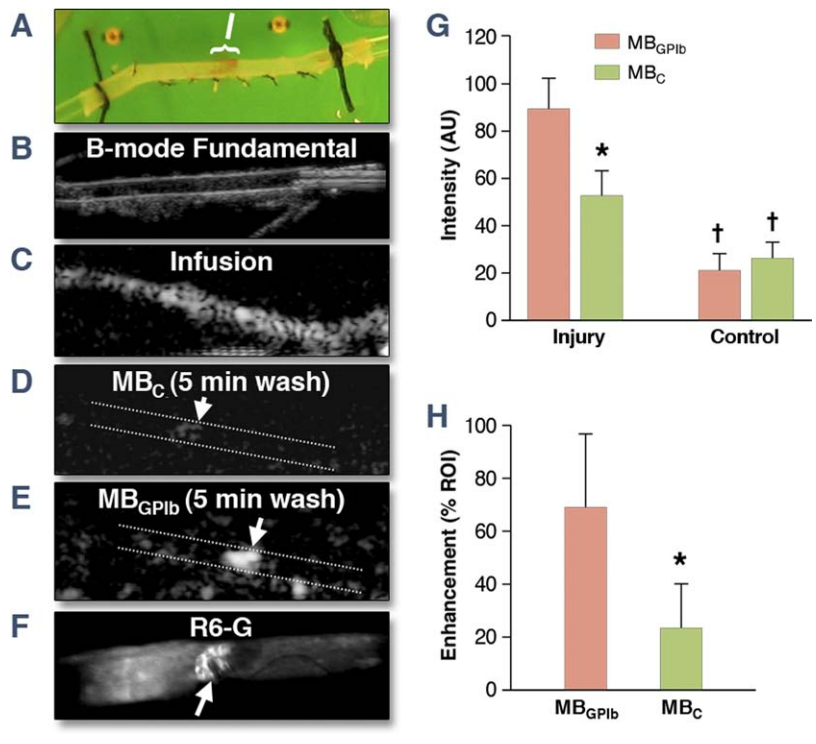

Figure 2. Targeted CEU Imaging of Ex Vivo Aortic Injury

Images show: **(A)** the ex vivo aorta after focal injury (I); **(B)** a high-resolution B-mode image; **(C)** contrast-enhanced ultrasound (CEU) during infusion of a microbubble agent; **(D)** CEU after control nontargeted microbubbles (MB_C) and wash; **(E)** CEU after von Willebrand factor–targeted microbubbles (MB_{GPIb}) and wash; and **(F)** fluorescent microscopy of an aortic whole mount illustrating rhodamine-6G–labeled platelet adhesion. **Arrows** denote the site of injury. **(G)** Mean (± standard error of the mean [SEM]) signal enhancement measured at the injury or remote site. **(H)** Mean (± SEM) percentage of pixels within the injured territory that demonstrated enhancement on pixel-intensity threshold analysis. *$p < 0.05$ versus glycoprotein Ib agent; †$p < 0.05$ versus corresponding agent in the injured segment. AU = acoustic units; ROI = region of interest.

layer of thrombus covered 20% to 30% of the surface area after infusion with whole blood. Because of the coarse texture of thrombi on microscopy, fluorescent microscopy was used to evaluate adhesion of DiO- or dioctadecyltetramethylindocarbocyanine perchlorate–labeled microbubbles (Online Fig. 1). Adhesion of vWF-targeted microbubbles was >10-fold greater than that for control microbubbles, of which >80% was in the region of thrombus formation (Fig. 1). Immunohistochemistry revealed the presence of surface-bound vWF on the thrombi.

Ex vivo molecular imaging of vascular injury. In the ex vivo aortic injury studies (Fig. 2), signal from vWF-targeted microbubbles was approximately 4-fold greater at the injury site compared with the remote noninjured regions (Fig. 2). Some enhancement at the injury site was also seen for control nontargeted microbubbles, although significantly less than for the vWF-targeted preparation. The spatial extent of enhancement at the injury site determined by PITA was also greater for vWF-targeted versus control microbubbles. Fluorescent microscopy of aortic whole mounts demonstrated the presence rhodamine-6G–labeled platelet adhesion at the site of injury, which was not observed in control experiments performed with nonspecific fluorescent antibody.

In vivo molecular imaging of atherosclerosis. On histology with Movat's pentachrome (Figs. 3A and 3B), there were advanced lumen-encroaching atherosclerotic lesions, often with necrotic cores, in all 40-week-old LDLR$^{-/-}$/ApoBec-1$^{-/-}$ mice, with a mean transaxial plaque area of 116,557 ± 78,303 μm^2. Atherosclerotic lesions were not observed in control wild-type mice. Endothelial vWF expression in LDLR$^{-/-}$/ApoBec-1$^{-/-}$ mice was particularly dense at sites overlying these severe atherosclerotic lesions (Fig. 3D). On molecular imaging of the aortic arch, the degree and percent area of enhancement for vWF-targeted microbubbles in the ascending aorta was greater in LDLR$^{-/-}$/ApoBec-1$^{-/-}$ mice relative to wild-type mice (Fig. 4). Signal was also greater for vWF-targeted compared with control microbubbles in LDLR$^{-/-}$/ApoBec-1$^{-/-}$ mice. On dual fluorescent microscopy, there was a significant nonlinear relationship between labeled platelets and labeled vWF-targeted microbubbles and on a per-optical field analysis (Fig. 5), yet there was little colocalization on a pixel-by-pixel basis, suggesting that platelets and vWF-targeted microbubbles adhered in the same regions but not to one another. Adhesion for both was greatest in regions of large plaques, and almost no adhesion was seen in wild-type mice. Scanning electron microscopy of the luminal surface demonstrated severe lesion formation in LDLR$^{-/-}$/ApoBec-1$^{-/-}$ mice (Fig. 6). On the surface of these lesions, there were large regions where leukocyte and platelet adhesion to the intact endothelial surface was seen. Although uncommon, there were also occasional focal endothelial erosions with overlying fibrin, platelets, and leukocytes.

DISCUSSION

The endothelium plays a pivotal role in maintaining normal vascular homeostasis. In atherosclerosis, loss of normal endothelial function includes the transition from an antithrombotic to a prothrombotic and proinflammatory state, with increased focal platelet adhesion and aggregation and eventual loss of endothelial barrier in regions of erosion or rupture (10). In this study, our aim was to test whether molecular imaging of the activated form of vWF could be used to detect these processes. Contrast

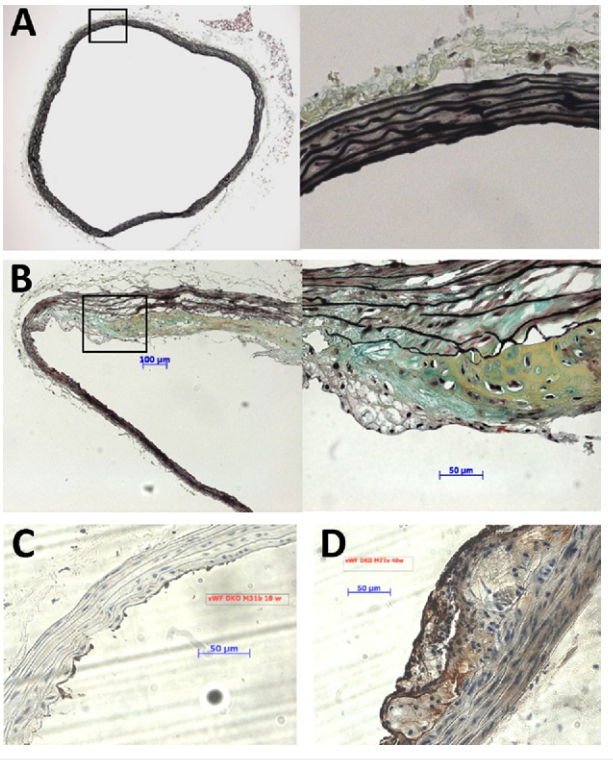

Figure 3. Aortic Histology and Immunohistochemistry

Movat's pentachrome stain illustrating normal aorta from a wild-type mouse **(A)** and severe lesion formation in a low-density lipoprotein receptor, Apobec-1–deficient (LDLR$^{-/-}$/ApoBec-1$^{-/-}$) mouse **(B)**. Immunohistochemistry of von Willebrand factor (vWF) from a wild-type mouse **(C)** and an LDLR$^{-/-}$/ApoBec-1$^{-/-}$ mouse **(D)**, the latter showing dense staining at the endothelial surface.

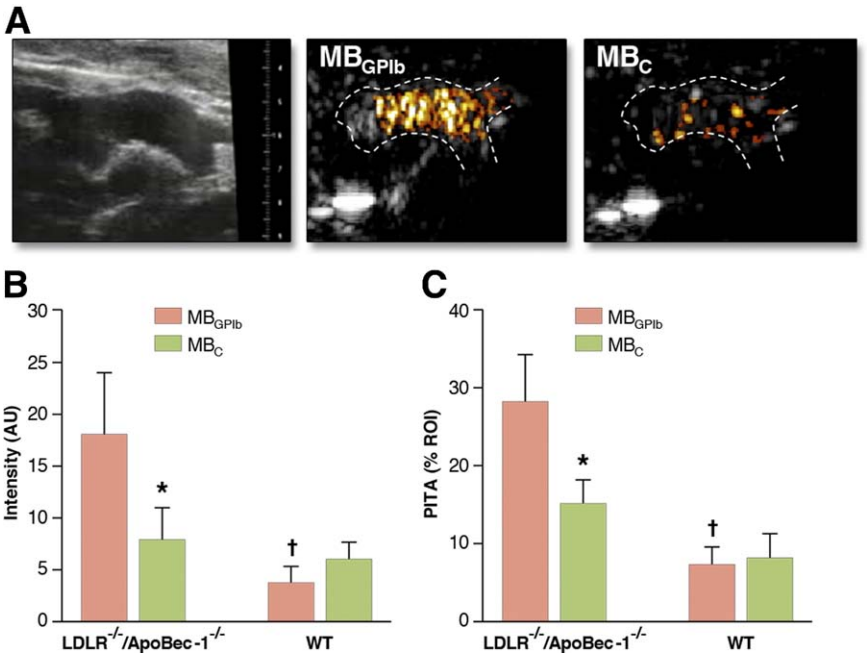

Figure 4. Molecular Imaging of vWF in Wild-Type and LDLR$^{-/-}$/ApoBec-1$^{-/-}$ Mice

(A) Images are of the aortic arch from a single LDLR$^{-/-}$/ApoBec-1$^{-/-}$ mouse illustrating marked thickening of the less curvature of the aorta and at the origin of the brachiocephalic vessel on B-mode imaging **(left)** and background-subtracted color-coded contrast ultrasound images after injection of either vWF-targeted (MB_{GPIb}) or control (MB_c) microbubbles. **(B)** Mean (± standard error of the mean [SEM]) signal enhancement from the aorta. **(C)** Mean (± SEM) percentage of pixels within the injured territory that demonstrated enhancement on pixel-intensity threshold analysis. *p < 0.05 versus glycoprotein Ib agent; †p < 0.05 versus LDLR$^{-/-}$/ApoBec-1$^{-/-}$. Abbreviations as in Figures 2 and 3.

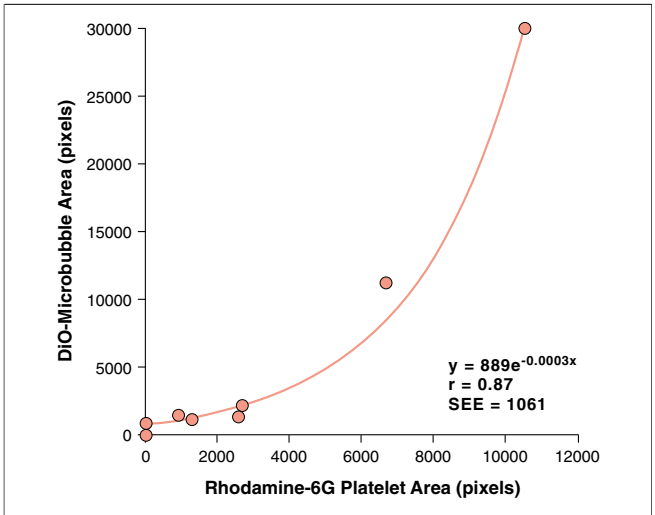

Figure 5. Spatial Relation Between Platelet and vWF-Targeted Microbubble Adhesion

Relation between number of fluorescent pixels per identical optical field (0.05 mm^2) on microscopy of rhodamine-6G–labeled platelets and dioctadecyloxacarbocyannine perchlorate (DiO)–labeled vWF-targeted microbubbles. The data point at the origin (0 pixels for platelets and microbubbles) represented 9 separate measurements from a wild-type mouse. Abbreviation as in Figure 1.

ultrasound imaging with microbubbles bearing recombinant GPIbα detected a high-risk atherosclerotic phenotype manifest by loss of endothelial antithrombotic function and occasional endothelial erosion.

For imaging in this study, we used "platelet mimicry" in the form of microbubbles bearing the GPIbα subunit to detect the presence of activated vWF in advanced spontaneous atherosclerosis. Interaction between GPIb and vWF is a high-affinity event that occurs early in thrombus formation and can support cell recruitment even in the face of high wall shear rates (2,11). Molecular imaging with GPIb as a targeting moiety is, therefore, well-suited to the large vessels of interest when imaging atherothrombotic events with particle-based contrast agents. Moreover, competitive inhibition from vWF in the blood pool is unlikely to be a major obstacle because the A1-domain is cryptic under static conditions and becomes available for GPIb binding when vWF is matrix-associated or multimerized (1,11). Hence our approach could be more sensitive and less prone to problems with competitive inhibition than other thrombus-targeted molecular imaging strategies that

have relied on targeting fibrin or platelet GPIIb/IIIa receptors (12,13).

The flow chamber and ex vivo aorta protocols in this study confirmed specific binding of our probe to vWF in shear flow. In the former, there was colocalization of vWF on immunostaining and targeted microbubble attachment, which occurred primarily where there were also platelets. This finding suggested competition of GPIbα-bearing microbubbles and platelets for the same vWF-rich regions. It is also possible that GPIbα microbubbles attached to vWF that had adhered to platelets via non–A1-domain mechanisms such as through GPIIb/IIIa (14). In the ex vivo aorta studies, CEU signal enhancement was greatest for vWF-targeted microbubbles at the injury site. Some selective enhancement at the injury site was also seen for control microbubbles, which was likely caused by either fibrin mesh entrapment of microbubbles or nonspecific attachment to leukocytes (15) that also are incorporated in these microthrombi (Fig. 7).

In LDLR$^{-/-}$/ApoBec-1$^{-/-}$ mice, the integration of histology and CEU data indicated that molecular imaging of activated vWF could detect high-risk features of advanced atherosclerotic disease. On electron microscopy, regions of endothelial erosion with platelet adhesion were sparse and therefore unlikely to account for the diffuse vWF-targeted signal enhancement. Regions of dense platelet adhesion and platelet-leukocyte complexes on the plaque endothelial surface were much more common and have been described in other animal models of atherosclerosis (4,5). En face dual fluorescent microscopy indicated that microbubbles attached in these areas where platelet adhesion was dense, but did not attach to platelets themselves. This observation suggests the presence of microdomains of activated vWF on the endothelial surface, which has also been noted in lesion-prone regions in hypercholesterolemic rabbits where platelets accumulate (4).

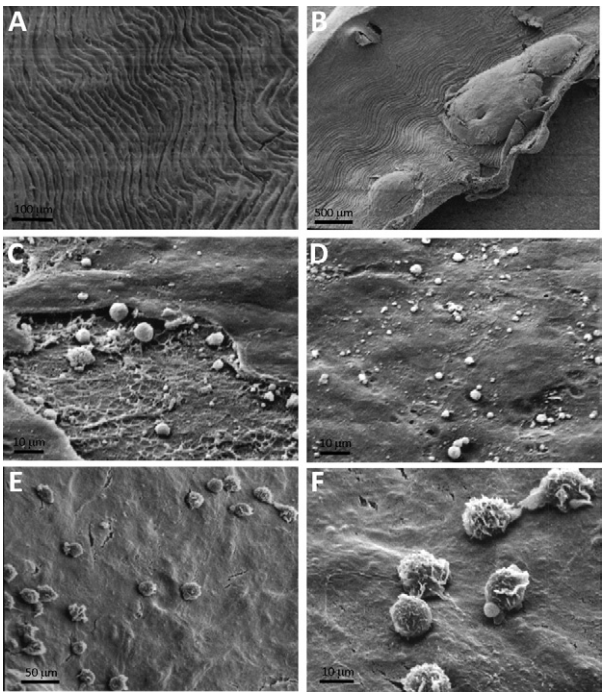

Figure 6. Scanning Electron Microscopy of the Luminal Aortic Surface

(A) Normal aortic surface from a wild-type mouse. **(B)** LDLR$^{-/-}$/ApoBec-1$^{-/-}$ aorta demonstrating multiple large protruding plaques. High-magnification images from the plaque surface of LDLR$^{-/-}$/ApoBec-1$^{-/-}$ mice demonstrated **(C)** small regions of erosions with overlying fibrin and platelets, **(D)** platelet adhesion to the intact endothelial surface, and **(E)** leukocyte adhesion to the endothelial surface, including **(F)** occasional platelet-leukocyte complexes. Abbreviation as in Figure 3.

The notion that endothelial vWF in atherosclerosis is surface-bound, activated, and amenable to interaction with the GPIbIX-V complex has not been fully explored in terms of its importance to plaque growth or instability. vWF is secreted from Weibel-Palade bodies and can remain associated with the endothelium after release (16). Subsequent

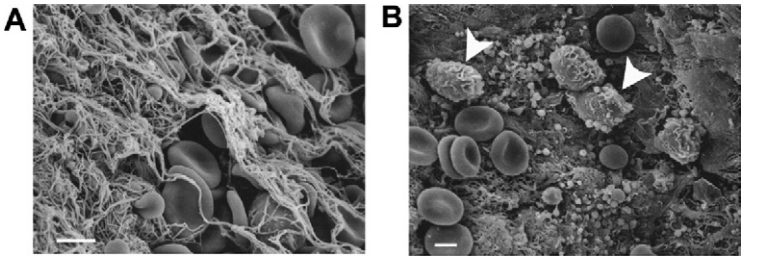

Figure 7. Scanning Electron Microscopy of Murine Thrombus

Images illustrate the complex macromolecular and cellular elements of thrombus, including **(A)** the fibrin entrapment of erythrocytes, and **(B)** platelets and the presence of leukocytes **(arrowheads)**. Scale bar = 5 μm.

multimerization of vWF is normally regulated by the proteolytic activity of a disintegrin and metalloproteinase with thrombospondin motifs-13. Because reduced activity of a disintegrin and metalloprotease with thrombospondin motifs-13 has been associated with advanced atherosclerotic disease (3,17), it is possible that dysregulated vWF multimerization was responsible for focal attachment of platelets and targeted microbubbles rather than upregulation alone. Alternatively, abnormal shear forces in regions of plaque could also have contributed to vWF activation and GP1bα-mediated attachment.

Our data suggest that molecular imaging of vWF could be used not only to detect a prothrombotic state, but also to detect a heightened inflammatory state. Brief platelet interactions with endothelial cells have been shown to potentiate the atherosclerotic lesion development through the deposition of chemokines on the endothelial surface (5). Targeted imaging of surface-bound activated vWF may be a means to detect endothelial activation in early or late atherosclerosis, similar to what has been shown for P-selectin, which is also stored within the endothelial Weibel-Palade bodies (18).

There are several limitations of this study that deserve attention. We have not fully characterized the relation between shear and vWF-targeted microbubble attachment, which could be important in atherosclerotic lesions where shear heterogeneity is expected. We have also not definitively shown that GPIbα binding to the A1 domain of vWF was the only mechanism involved in microbubble attachment in atherosclerotic mice because GPIb can interact with other endothelial and leukocyte surface proteins (1). There is no gold standard for quantifying endothelial luminal vWF and differentiating this from normal synthesis and storage. However, this limitation also highlights the uniqueness of molecular imaging with an intravascular probe that will only be retained if counter ligand is encountered within the vascular lumen. It is also worth noting that nontargeted microbubbles resulted in higher signals in $LDLR^{-/-}$/ApoBec-$1^{-/-}$ versus wild-type mice. The mechanism for this phenomenon, which we have encountered in almost all CEU molecular imaging studies of inflammatory conditions, is most likely from complement-mediated attachment to leukocytes on the plaque surface (15).

CONCLUSIONS

In summary, we have demonstrated that advanced atherosclerotic disease with high-risk features can be detected by molecular imaging of activated vWF. Our results support the further exploration of vWF as a molecular imaging target for differentiating atherosclerotic risk and possibly for the detection of key events that occur during atherothrombotic complications.

Reprint requests and correspondence: Dr. Jonathan R. Lindner, Cardiovascular Division, UHN-62, Oregon Health & Science University, 3181 SW Sam Jackson Park Road, Portland, Oregon 97239. *E-mail: lindnerj@ohsu.edu.*

REFERENCES

1. Ruggeri ZM. Platelets in atherothrombosis. Nat Med 2002;8:1227–34.
2. Yago T, Lou J, Wu T, et al. Platelet glycoprotein 1bα forms catch bonds with human WT vWF but not with type 2B von Willebrand disease vWF. J Clin Invest 2008;118:3195–207.
3. Kaikita K, Soejima K, Matsukawa M, Nakagaki T, Ogawa H. Reduced von Willebrand factor-cleaving protease (ADAMTS13) activity in acute myocardial infarction. J Thromb Haemost 2006;4:2490–3.
4. Theilmeier G, Michiels C, Spaepen E, et al. Endothelial von Willebrand factor recruits platelets to atherosclerosis-prone sites in response to hypercholesterolemia. Blood 2002;99:4486–93.
5. Huo Y, Schober A, Forlow SB, et al. Circulating activated platelets exacerbate atherosclerosis in mice deficient in apolipoprotein E. Nat Med 2003;9:61–7.
6. Lindner JR, Song J, Christiansen J, Klibanov AL, Xu F, Ley K. Ultrasound assessment of inflammation and renal tissue injury with microbubbles targeted to P-selectin. Circulation 2001;104:2107–712.
7. Berny MA, White TC, Tucker EI, et al. Thrombin mutant W215A/E217A acts as a platelet GPIb antagonist. Arterioscler Thromb Vasc Biol 2008;28:329–34.
8. Micari A, Sklenar J, Belcik JT, Kaul S, Lindner JR. Automated detection of the spatial extent of perfusion defects and viability on myocardial contrast echocardiography. J Am Soc Echocardiogr 2006;19:379–85.
9. Powell-Braxton L, Veniant M, Latvala RD, et al. A mouse model of human familial hypercholesterolemia: markedly elevated low density lipoprotein cholesterol levels and severe atherosclerosis on a low-fat chow diet. Nat Med 1998;4:934–8.
10. Libby P. The molecular mechanisms of the thrombotic complications of atherosclerosis. J Intern Med 2008;263:517–27.
11. Andrews RK, Berndt MC. Platelet adhesion: a game of catch and release. J Clin Invest 2008;118:3009–11.
12. Nahrendorf M, Sosnovik DE, French B, et al. Multimodality cardiovascular molecular imaging; Part II. Circ Cardiovasc Imaging 2009;2:56–70.
13. Hamilton AJ, Huang SL, Warnick D, et al. Intravascular ultrasound molecular imaging of atheroma components in vivo. J Am Coll Cardiol 2004;43:453–60.

14. Ruggeri ZM, De Marco L, Gratti L, Bader R, Montgomery RR. Platelets have more than one binding site for von Willebrand factor. J Clin Invest 1983;72:1–12.
15. Lindner JR, Coggins MP, Kaul S, et al. Microbubble persistence in the microcirculation during ischemia-reperfusion and inflammation: integrin- and complement-mediated adherence to activated leukocytes. Circulation 2000; 101:668–75.
16. Dong JF, Moake JL, Nolasco L, et al. ADAMTS-13 rapidly cleaves newly secreted ultralarge von Willebrand factor multimers on the endothelial surface under flowing conditions. Blood 2002;100:4033–9.
17. Bongers TN, de Bruijne ELE, Dippel DWJ, et al. Lower levels of ADAMTS13 are associated with cardiovascular disease in young patients. Atherosclerosis 2009;207:250–4.
18. Kaufmann B, Carr CL, Belcik JT, et al. Molecular imaging of the initial inflammatory response in atherosclerosis: implications for early detection of disease. Arterioscler Thromb Vasc Biol 2009;30:54–9.

Key Words: atherosclerosis ■ microbubble ■ molecular imaging ■ von Willebrand factor.

▶APPENDIX

For supplementary figures, please see the online version of this article.